A Mixed Fullerene–Ferrocene Thermotropic Liquid Crystal: Synthesis, Liquid-Crystalline Properties, Supramolecular Organization and Photoinduced Electron Transfer

Michaël Even,[a] Benoit Heinrich,[b] Daniel Guillon,*[b] Dirk M. Guldi,*[c] Maurizio Prato,*[d] and Robert Deschenaux*[a]

Dedicated to Professor Fred Wudl on the occasion of his 60th birthday

Abstract: Grafting of a ferrocene-containing liquid-crystalline malonate derivative to C_{60} led to the mixed fullerene–ferrocene material **1** which gave rise to a smectic A phase. Cholesterol was used as liquid-crystalline promoter. X-ray diffraction experiments and volumetric measurements indicated that **1** is organized in double layered structures. The corresponding supramolecular organization within the mesomorphic lamellar phase is characterized by a microsegregation of the different units (ferrocene, fullerene, and cholesterol) in distinct sublayers. In such a smectic A phase, C_{60} imposes the arrangement of the other molecular moieties. Photophysical studies revealed that electron transfer occurs from the donor ferrocene to the electron accepting fullerene. The formation of a long-lived radical pair, with lifetimes of the order of several hundred nanoseconds, was confirmed by time-resolved spectrometry, especially in the near infrared region, in which the radical anion of the fullerene moiety displays its characteristic fingerprint absorption.

Keywords: electron transfer · ferrocene · fullerenes · liquid crystals · materials science

Introduction

[60]Fullerene (C_{60}) has attracted considerable attention in materials science.[1] The possibility to develop materials possessing the unique properties of C_{60} motivated these studies. In particular, C_{60} has been incorporated into polymers,[2] dendrimers,[3] sol–gel matrices[4] and nanospheres.[5] Much research has also been devoted to the synthesis and photophysical studies of systems in which C_{60} behaves as an energy/electron acceptor in the ground or excited state[6] either in covalently linked dyads[7] or as heterogeneous blends[8] for the fabrication of photovoltaic devices.[9] Recently, C_{60} was used to construct a single layer organic LED.[10]

The search for fullerene-based materials prompted us to investigate fullerene-containing thermotropic liquid crystals.[11–14] Our concept, the use of liquid-crystalline malonates in the Bingel reaction,[15] led to mesomorphic mono-[11–13] and hexa-[14] adducts of C_{60}. The mono-adducts were prepared from an organic-type malonate,[11] a ferrocene-containing malonate,[12] and a ferrocene-based dendritic malonate.[13] In these compounds, cholesterol was used as the liquid-crystalline promoter. The hexa-adduct[14] was prepared from a malonate containing cyanobiphenyl groups, the latter acting as mesogenic fragments. The C_{60} derivatives gave rise to smectic A phases, and showed good thermal stability and good solubility in common organic solvents. Besides our work, two reports described liquid-crystalline fullerenes exhibiting either calamitic[16] or cubic[17] phases.

The fullerene–ferrocene derivative **1** (Scheme 1) was designed to develop photoactive liquid crystal switches by combining two sets of data: firstly, electron transfer was used to generate liquid-crystalline ferrocenium derivatives from non-mesomorphic ferrocenes,[18] and, secondly, photoinduced electron transfer from ferrocene to C_{60} was shown to occur in fullerene–ferrocene dyads.[19] Therefore, photoinduced electron transfer in fullerene–ferrocene liquid crystals could be

[a] Prof. R. Deschenaux, M. Even
Institut de Chimie, Université de Neuchâtel, Avenue de Bellevaux 51
Case postale 2, 2007 Neuchâtel (Switzerland)
Fax: (+41) 32 718 25 11
E-mail: robert.deschenaux@unine.ch

[b] Dr. D. Guillon, Dr. B. Heinrich
Institut de Physique et Chimie des Matériaux de Strasbourg
Groupe des Matériaux Organiques
23, rue du Loess, 67037 Strasbourg Cedex (France)

[c] Prof. D. M. Guldi
University of Notre Dame, Radiation Laboratory
Notre Dame, Indiana 46556 (USA)

[d] Prof. M. Prato
Dipartimento di Scienze Farmaceutiche, Università di Trieste
Piazzale Europa 1, 34127 Trieste (Italy)

  0947-6539/01/0712-2595 $ 17.50+.50/0

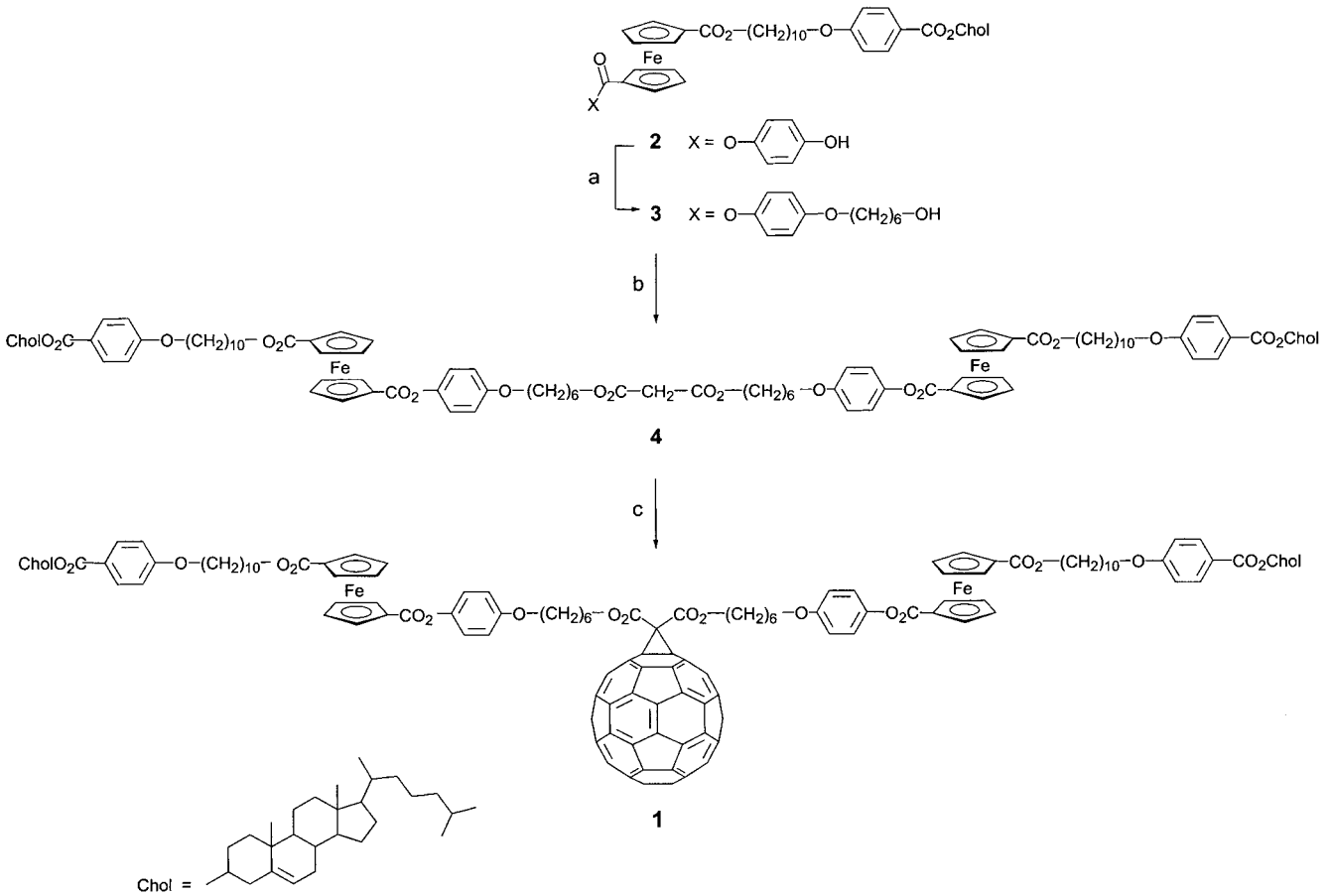

Scheme 1. a) 6-Bromohexanol, K_2CO_3, THF, 24 h, 36%. b) Malonyl chloride, triethylamine, CH_2Cl_2, 2 h, 77%. c) [60]Fullerene, diazabicyclo[5.4.0]undec-7-ene (DBU), iodine, toluene, 3 h, 34%.

used to control the liquid-crystalline properties because of the presence of either the ferrocene (light off) or ferrocenium (light on) species.

The development of switchable liquid crystals based on C_{60} and ferrocene is a difficult task since several parameters, ranging from structure and liquid-crystalline properties to photophysical behavior, are involved. The synthesis and study of various derivatives are required to understand their photophysical properties in connection with their liquid-crystalline behavior. Compound **1** represents the first member of this class of materials and can be considered as a prototype from which other derivatives will be constructed. A detailed investigation of its properties is expected to bring important insights for the design of further compounds.

We describe, herein, the synthesis, liquid-crystalline properties and supramolecular organization of **1** and of its intermediates, as well as the photoinduced electron transfer of **1** in organic solvents. The general synthetic strategy for **1** and its mesomorphic behavior have been reported elsewhere.[12]

Results and Discussion

Synthesis: The synthesis of **1** is shown in Scheme 1. O-Alkylation of phenol derivative **2**[13] with 6-bromohexanol gave alcohol intermediate **3**, which was esterified with malonyl chloride to furnish the malonate derivative **4**. Addition of the latter to C_{60} gave the targeted compound **1**. Compounds **5** ($n = 8$, 12, 14) were prepared as shown in Scheme 2 by O-alkylation of cholesteryl 4-hydroxybenzoate[20] (**6**) with the appropriate 1-bromoalkane; they were prepared to determine the molecular volume of the cholesterol moiety by volumetric methods.

Liquid-crystalline properties: The mesomorphic and thermal properties of **1**–**5** were investigated by polarized optical

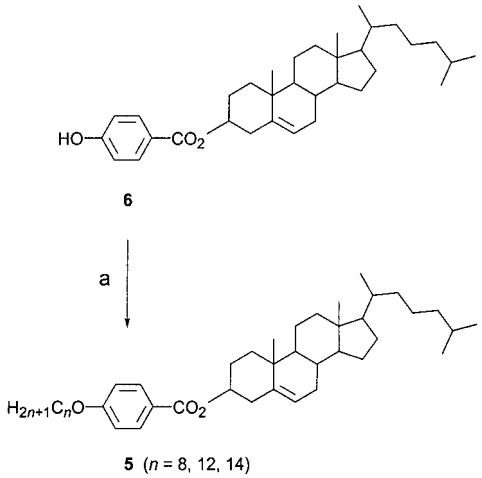

Scheme 2. Different *n*-bromoalkanes, K_2CO_3, DMF/THF, 120°C.

0947-6539/01/0712-2596 $ 17.50+.50/0 *Chem. Eur. J.* **2001**, *7*, No. 12

microscopy (POM), differential scanning calorimetry (DSC) and X-ray diffraction (XRD). The phase transition temperatures and enthalpies are reported in Table 1.

Compounds **1**–**4** gave smectic A phases. An additional chiral nematic phase (cholesteric phase) was observed for **3**.

Table 1. Phase transition temperatures and enthalpy changes of compounds **1**–**5**.

Compound	Transition[a]	Temperature [°C]	ΔH [kJ mol^{-1}]
2	Cr–S_A[b]	112	6.5
	S_A–I	151	3.1
3	Cr–S_A[b]	63	15.1
	S_A–N*	125	–[c]
	N*–I	127	2.9[c]
4	Cr–S_A[b]	73	80.6
	S_A–I	134	6.4
1	Cr–S_A[b]	66	12.9
	S_A–I	118	11.7
5 ($n=8$)[d]	Cr–S_A	136	33.6
	S_A–N*[e]	173	–
	N*–I	218	1.0
5 ($n=12$)	Cr–S_A	127	32.5
	S_A–N*	176	0.7
	N*–I	198	0.7
5 ($n=14$)	Cr–S_A	115	28.1
	S_A–N*	175	1.1
	N*–I	189	1.1

[a] Cr = crystal, S_A = smectic A phase, N* = chiral nematic (cholesteric) phase, I = isotropic fluid. [b] Observed during the first heating run. [c] Peak overlap. The enthalpy value corresponds to the sum of both enthalpies. [d] A monotropic phase might form below the smectic A phase. This behavior was not investigated. [e] Observed by polarized optical microscopy.

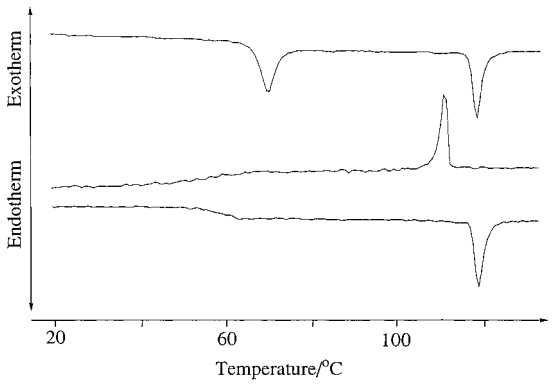

Figure 1. Differential scanning calorimetry thermogram of **1** recorded during the first heating (top), first cooling (middle), and second heating (bottom) run.

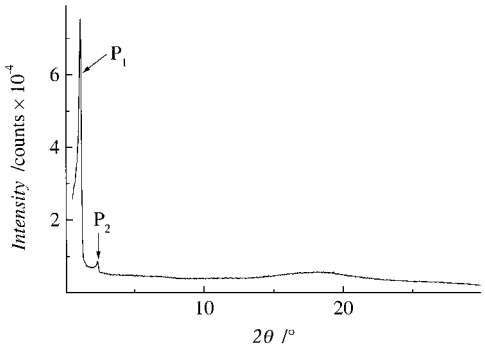

Figure 2. Representative X-ray diffraction pattern of **1** recorded at 110 °C. P_1 and P_2 refer to the first and second order signals corresponding to the layer periodicity. The diffuse signal at large angles corresponds to the liquid-like arrangement of the molecules within the smectic layers.

The liquid-crystalline phases were identified by POM: the smectic A phases gave focal-conic and homeotropic textures, and the cholesteric phase gave the plane texture. Identification of the liquid-crystalline phase displayed by **1** was more difficult; because of higher viscosity than the fullerene-free compounds **2**–**4**, small focal conics appeared only when the sample was cooled very slowly from the isotropic fluid.

By DSC, the melting points of **1**–**4** were detected during the first heating run only. From the first cooling run, a glass transition temperature was recorded revealing a low tendency of **1**–**4** to recrystallize under the experimental conditions applied. The low enthalpy value associated with the melting process observed for **1**–**3** was an indication of a semicrystalline nature of the samples. The DSC traces of **1** are shown in Figure 1.

The nature of the smectic A phase of **1**–**4** was confirmed by XRD. Diffraction patterns typical of disordered smectic phases were registered. In the low-angle region, they consisted of two sharp diffraction peaks, the corresponding spacings of which are in a 1:2 ratio, and in the wide-angle region, of a diffuse signal. A representative diffractogram of **1** is shown in Figure 2.

The dependence of the *d*-layer spacing as a function of temperature was determined for **1**–**4** (Figure 3). Interestingly, $d = f(T)$ did not follow the typical variation observed for the smectic A phase for which a decrease of the *d*-layer spacing is observed with increasing temperature. Here (Figure 3), the

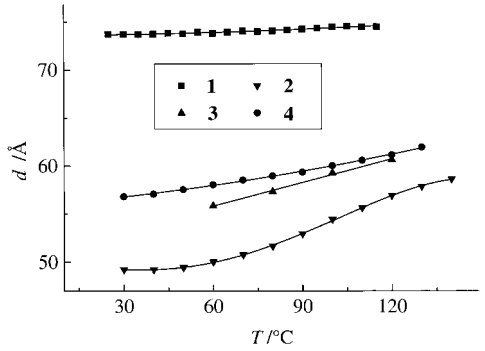

Figure 3. Dependence of the layer periodicity of **1**–**4** measured as a function of temperature.

d-layer spacing either increased for compounds **2**–**4** or remained nearly constant as for **1** when the temperature was raised. For each compound, the *d*-layer spacing was determined at 80 °C and compared with the molecular length estimated by Corey–Pauling–Koltun (CPK) space-filling molecular models in the fully extended conformation (Table 2).

The *d*-layer spacing values found for **2** and **3** were close to their molecular lengths which led to d/L ratios of 1.00 and 0.97 for **2** and **3**, respectively. The *d*-layer spacing values found for **4** and **1** were smaller than their molecular lengths and gave d/L ratios of 0.49 and 0.62 for **4** and **1**, respectively.

The increase of *d* observed on going from **4** to **1**, that is upon addition of C_{60} to **4**, should reflect a different supramolecular

Table 2. Layer spacing and approximate molecular length of compounds **1**–**5**.

Compound	d [Å][a]	L [Å][b]	d/L
2	51.6[c]	51.3	1.00
3	57.3[c]	58.8	0.97
4	58[c]	119.5	0.49
1	74.1[c]	118.6	0.62
5 ($n=8$)	32.6[d]	36.1	0.90
5 ($n=12$)	37.1[d]	41.1	0.90
5 ($n=14$)	39.4[d]	43.6	0.90

[a] Determined by X-ray diffraction. [b] Estimated by Corey–Pauling–Koltun (CPK) space filling molecular models in the extended molecular conformation. [c] At 80 °C. [d] At 150 °C.

organization of **4** and **1** within the liquid-crystalline phase. Indeed, the molecular length of **1** and **4** are almost identical (Table 2).

Supramolecular organization: To describe the molecular organization within the smectic A layers, it is necessary to take into account the fact that the different molecular moieties, which form such a large molecule as **1**, have quite different cross-sectional areas. For example, the molecular areas of C_{60} and classical mesogenic groups are about 100[21] and 25[22] Å^2, respectively, whereas that of ferrocene is close to 44 Å^2.[23] As for the cholesterol moiety, it was decided to perform XRD and dilatometry experiments on the cholesterol derivatives **5** ($n=8$, 12, 14) to determine its cross-sectional area. Indeed, compounds **5** ($n=8$, 12, 14) show smectic A and cholesteric phases (Table 1), and therefore can be regarded as ideal candidates for such a purpose: in the smectic A phase, the cross-sectional area corresponds to the molecular area determined experimentally, since the molecules are normal to the layers.

The variation of the d-layer spacing as a function of temperature in the smectic A phase for compounds **5** ($n=8$, 12, 14) is shown in Figure 4. There is a slight decrease of d with

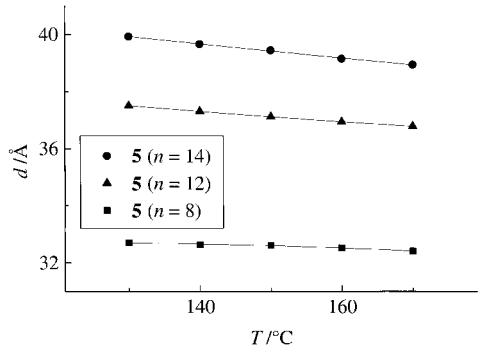

Figure 4. Dependence of the layer periodicity of **5** as a function of temperature in the smectic A phase.

increasing temperature. Such a behavior is usual in the case of smectic A phases and corresponds to an increase of the lateral distances between the molecules together with a spreading of the aliphatic chains at the interface between the layers. This spreading induces a decrease of the aliphatic sublayer thickness and, therefore, of the d value itself. Interestingly, the d values are close to those of the molecular lengths L calculated for stretched conformation of the molecules (Table 2). Moreover, the variation of d is linear with n, with an increase of 1.15 ± 0.05 Å per methylene group. This value is close to that expected for a completely stretched conformation of the chains (1.27 Å) and indicates that the chains are, on average, almost normal to the smectic layers.

Dilatometry measurements have been performed on compounds **5** ($n=8$, 12); as for **5** ($n=14$), the molecular volume V_m has been calculated by additivity of the values of V_m obtained for **5** ($n=12$) with those of the known values of methylene groups in the smectic A phase. When combining the data thus obtained with those of the layer spacing obtained by XRD, it is possible to deduce the molecular area S occupied by one molecule in the plane of the layers with $S = V_m/d$. This parameter is quite important to describe the molecular arrangement within the layers.[24] In Figure 5, the

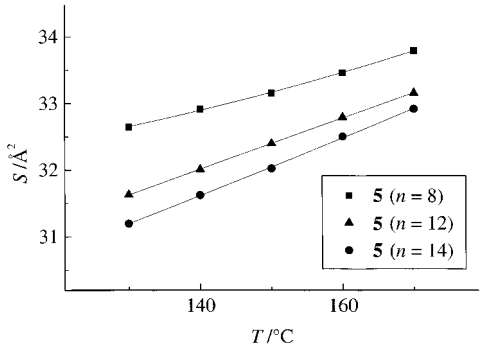

Figure 5. Dependence of the molecular area S of **5** as a function of temperature in the smectic A phase.

values of S are plotted as a function of temperature. Overall, the molecular area has values between 31 and 34 Å^2 and increases linearly with the temperature. These values are slightly smaller than those found for octylcholestane (37.7 Å^2 at 50 °C),[25] but are close to that found for the cholestane moiety estimated by molecular models ($\sigma \approx 34$ Å^2). They indicate that the smectic A layers of **5** are mainly monolayers (Figure 6): The cholesterol moieties form a monomolecular sublayer with the aliphatic chains rejected on each side of the sublayer. Since the molecular area found is much larger than the lateral bulkiness of a stretched melted aliphatic chain ($\sigma_{ch} \approx 23 \pm 0.7$ Å^2 at 130 °C), it can be concluded that the chains are highly disorganized.

Let us now consider compounds **1**–**4**. Their molecular volumes have been determined by using the additivity rule of the partial molecular volumes found by dilatometry experiments performed on **5** ($n=8$, 12) and 1,1′-dioctylferrocene,[23] and by using calculated values obtained from molecular models (using crystallographic data and Biosym software). All of the partial volumes have been determined at 20 °C and then calculated as a function of temperature, assuming a volume expansion coefficient $\alpha = (1/V) \times (dV/dT) \approx 7 \times 10^{-4}$ K^{-1}, which is usually found for smectic A phases.[26] To make relevant comparisons with compounds **5**, we have represented in Figure 7 these molecular areas related to the number of

0947-6539/01/0712-2598 $ 17.50+.50/0 *Chem. Eur. J.* **2001**, *7*, No. 12

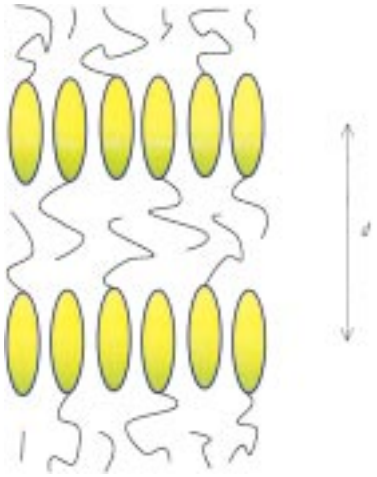

Figure 6. Proposed molecular organization of **5** in the smectic A layers. The ellipsoid parts and the wavy lines represent the cholesterol and aliphatic moieties, respectively.

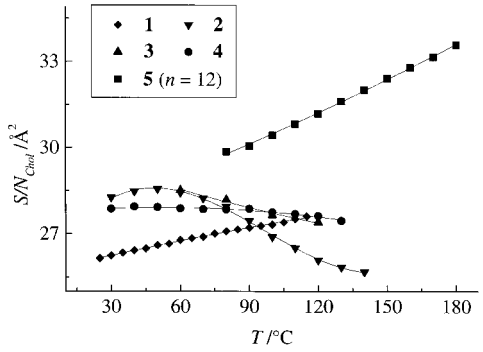

Figure 7. Dependence of the molecular area, normalized to the number of cholesterol moieties per molecule, of **1**–**5** as a function of temperature in the smectic A phase.

cholesterol moieties per molecule (S/N_{chol}) as a function of temperature. The values thus determined are close to those obtained for **5** at low temperature (if we consider the extrapolated values of **5** towards the lower temperatures), but become quite different at higher temperatures. This is in agreement with the increase of d as a function of temperature in the smectic A phase (Figure 3) reported above, and, most likely, due to a small rearrangement of the cholesterol moieties. In the low temperature range, the cholesterol moieties form a single-layered arrangement similar to that found for compounds **5**. When the temperature increases, the cholesterol moieties tend to form a slightly partial bilayered arrangement, resulting in an increase of d and a decrease of the molecular area S. It is important to point out that the intrinsic values of S, in the range between 25.5 and 28.5 Å^2, are significantly smaller than the cross-sectional area of the ferrocene moieties. This implies the models proposed in Figures 8 to 11.

In the case of compounds **2**–**4**, the molecular organization of one layer is characterized by three sublayers of different chemical nature and bulkiness segregating from one another and piling up one over the other to form the lamellar stacking of the smectic A phase. In the cholesteric sublayer, two adjacent cholesterol moieties occupy an average area of about

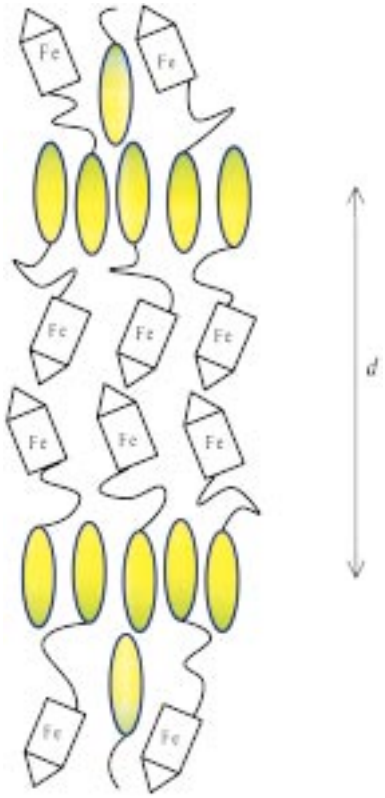

Figure 8. Proposed molecular organization of **2** in the smectic A layers. The ellipsoid parts and the wavy lines represent the cholesterol and aliphatic moieties, respectively.

55 Å^2, resulting from their partial bilayer arrangement, as explained above. In the ferrocene sublayer, the molecular area available for each group is thus 55 Å^2 and is larger than its natural bulkiness (≈45 Å^2 at 100 °C). Therefore, the ferrocene moieties are constrained to tilt with respect to the normal to the layers. However, there is no long range correlation of the tilt angle in order to keep the uniaxial property of the phase. In the aliphatic sublayers, the chains are spread over an area of 55 Å^2, which is more than twice the area occupied by a melted chain (≈23 Å^2 at 100 °C). This indicates that they are strongly disorganized and folded. For compounds **2** and **3**, possible hydrogen bonding between the hydroxy groups probably contribute to the stabilization of the layering.

In the case of **1**, there is a fourth sublayer constituted by the fullerene moieties. The cross-sectional area of C_{60} (≈100 Å^2) is about twice the area occupied by two adjacent cholesterol moieties. This implies that in order to describe the supramolecular organization, two molecules have to be taken into account in the elementary cell. The cholesterol, ferrocene, and aliphatic sublayers can be described as for compounds **2**–**4**. The fullerene moieties form a double sublayer inserted between aliphatic sublayers. In fact, the molecules organize themselves in double layers, where C_{60} plays the predominant role. Due to its large molecular area, C_{60} imposes the arrangement of the other molecular moieties. The space filling is thus obtained through a micro-segregation of the different molecular species together with a good adequacy between the interfaces of the different sublayers.

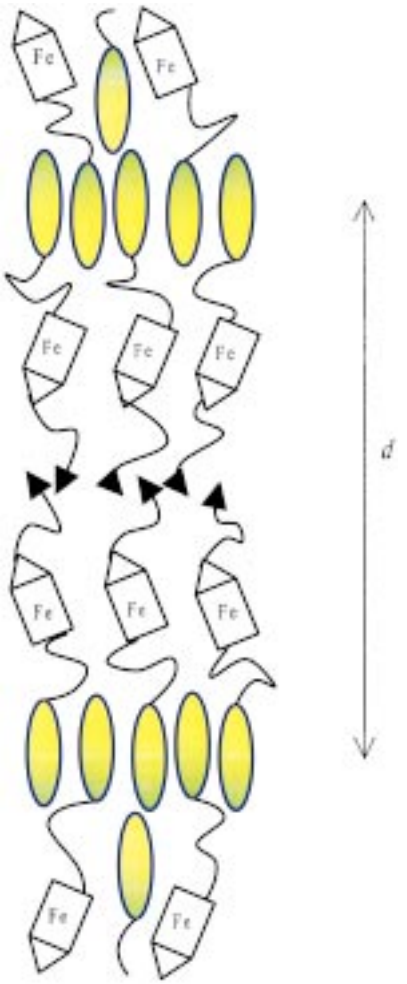

Figure 9. Proposed molecular organization of **3** in the smectic A layers. The ellipsoid parts and the wavy lines represent the cholesterol and aliphatic moieties, respectively.

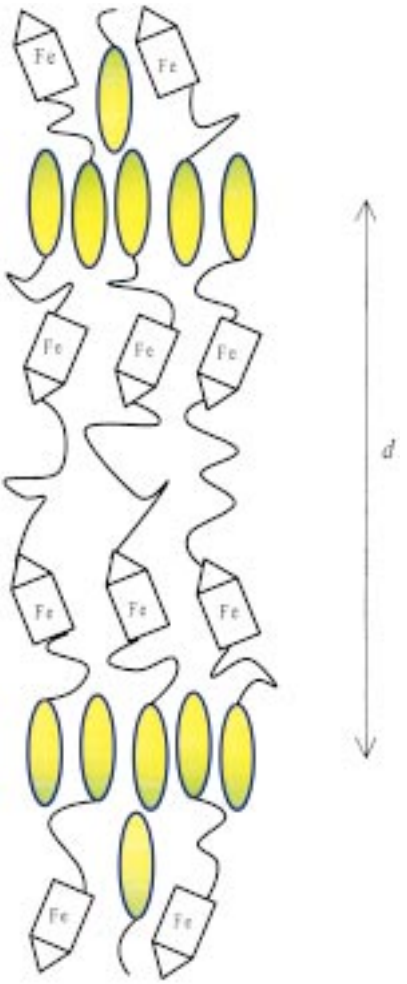

Figure 10. Proposed molecular organization of **4** in the smectic A layers. The ellipsoid parts and the wavy lines represent the cholesterol and aliphatic moieties, respectively.

Photophysical properties: Photoinduced phenomena including electron transfer (ET) in **1** were studied in solution by steady-state fluorescence and complemented by time-resolved transient absorption spectroscopy. The fluorescence of **1** and of the model diethylcarboxylate methanofullerene derivative **7** was taken in solvents of different polarity. The scope of these experiments was to measure the extent of fluorescence quenching in **1** relative to **7**, where the electron donating ferrocene moiety is absent. In addition, the increase in solvent polarity was meant to lower the energy of the charge-separated state and, in turn, to increase the free energy changes associated with the intramolecular ET event. This change in driving force is only made possible on the basis that the energy of the electron accepting state, namely the fullerene singlet state, remains independent of the solvent environment.

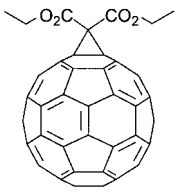

7

Emission spectra of the methanofullerene reference **7** in toluene and in benzonitrile at room temperature show the same maxima around 700 nm, with the same moderate yield of about 6.0×10^{-4}. This implies that the energy of the fullerene singlet excited state is not affected by the solvent polarity. In agreement with the hypothesis of an intramolecular ET between the electron donating ferrocene and the photoexcited fullerene, the fullerene fluorescence of **1** is indeed noticeably quenched in toluene relative to **7** (Table 3). Moreover, the fluorescence quantum yields are subject to a systematic decrease with the following order: toluene > THF > CH_2Cl_2 > benzonitrile (Figure 12).

Complementary fluorescence lifetime measurements (i.e., recording the fullerene emission at 700 nm) also reveal faster decay of the fullerene emission of **1** in all solvents investigated relative to reference **7** (Figure 13). Again, the lifetime decreased in the same order as derived from the steady-state emission experiments, namely toluene > THF > CH_2Cl_2 > benzonitrile (Table 3).

Considering the fluorescence measurements summarized above, an intramolecular ET can be inferred. To obtain direct spectroscopic evidence in support of this assumption, transient absorption spectra were acquired following either a 18 ps or a 6 ns laser pulse at 355 and 337 nm, respectively. In conjunction with the short laser pulses (i.e., 18 ps) the decay

  0947-6539/01/0712-2600 $ 17.50+.50/0

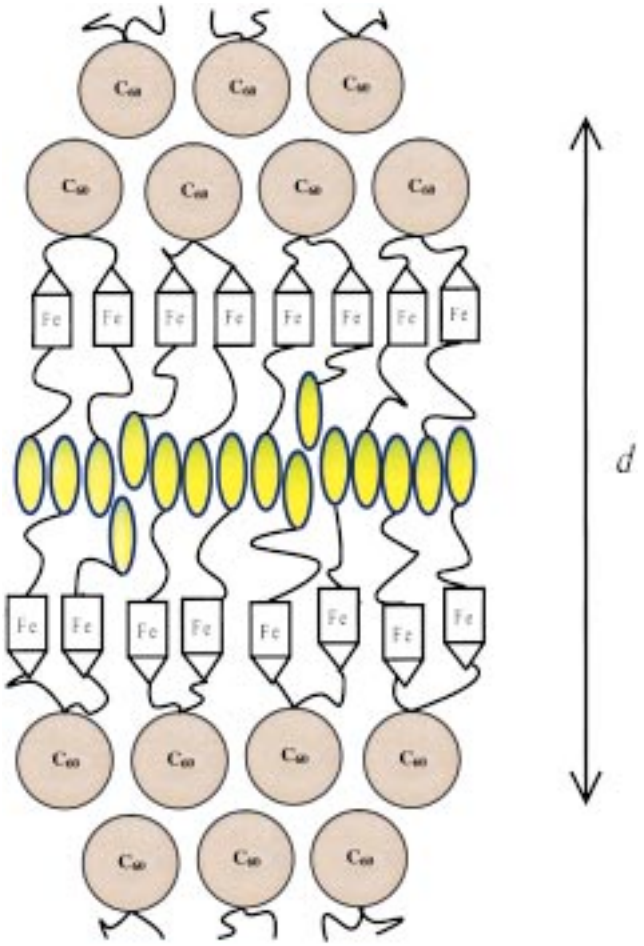

Figure 11. Proposed molecular organization of **1** in the smectic A layers. The ellipsoid parts and the wavy lines represent the cholesterol and aliphatic moieties, respectively.

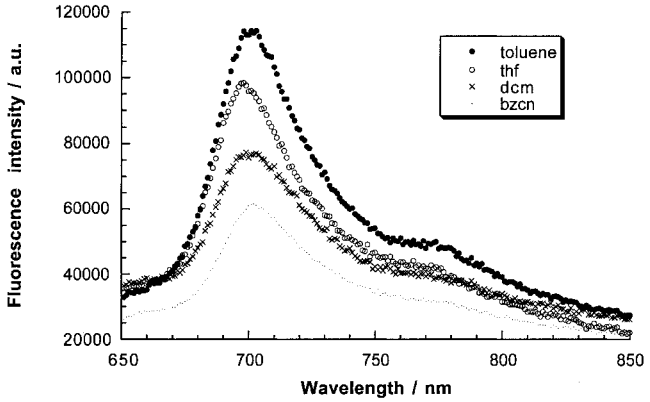

Figure 12. Steady-state fluorescence spectra of **1**. The absorbance of the solutions for the emission measurements was adjusted to 0.5 at the 335 nm excitation wavelength. (dcm = dichloromethane; bzcn = benzonitrile).

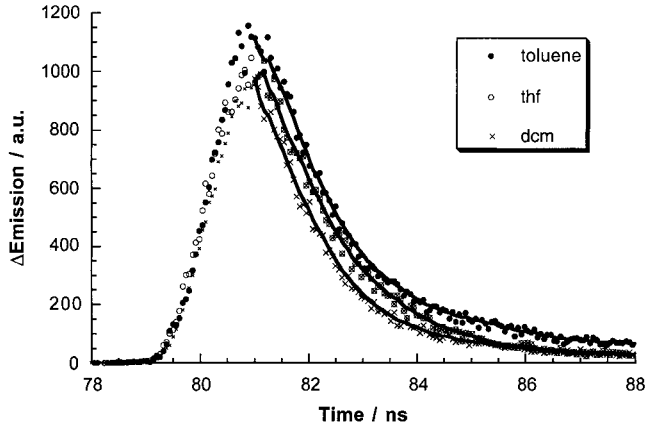

Figure 13. Fluorescence decay profiles of **1** ($\approx 5.0 \times 10^{-5}$ M) in deoxygenated solvents. (dcm = dichloromethane).

dynamics of the fullerene singlet excited state are probed in light of the forward ET. On the other hand, the longer laser pulses (i.e., 6 ns) are employed to shed light on the lifetime of the charge-separated state.

Table 3. Photophysical properties of compounds **1** and **7** in various organic solvents.

Solvent	Compound **1**					Compound **7**
	Dielectric constant [ε]	Fluorescence quantum yields (Φ)	Lifetime (τ) fluorescence [ns]	Lifetime (τ) singlet excited state [ns]	Lifetime (τ) radical pair [ns]	Fluorescence quantum yields (Φ)
toluene	2.39	4.4×10^{-4}	1.11	1.02		6.0×10^{-4}
THF	7.6	3.8×10^{-4}	1.07			6.0×10^{-4}
CH_2Cl_2	9.08	3.0×10^{-4}	0.81	0.72	27	5.8×10^{-4}
benzonitrile	24.8	2.2×10^{-4}	0.62	0.5	115	5.7×10^{-4}
benzonitrile/DMF	30.8				420	

In particular, picosecond excitation of the reference **7** reveals the following absorption characteristic: immediately after the laser pulse, a strong absorption was observed. A maximum around 920 nm is a clear fingerprint of the fullerene singlet–singlet absorption, which formation lies within the resolution of the applied laser pulses. The singlet excited state absorption decays with clean first order kinetics and a time constant of 6.5×10^8 s^{-1}. Simultaneously with the decay of the 920 nm absorption, a new transient grows in at around 720 nm. The decay and grow-in kinetics are in reasonably good agreement, which leads to the conclusion that a spin-forbidden intersystem crossing (ISC) governs the fate of the singlet excited state. This allows the assignment of the 720 nm absorption maximum to the triplet–triplet absorption. Further evidence for the transformation of the singlet excited state (1.77 eV) to the energetically lower lying triplet excited state (1.50 eV) stems from the presence of an isosbestic point at around 735 nm. It should be noted that the triplet excited state exhibits another maximum around 360 nm, which is, however, outside the detectable wavelength range of our picosecond apparatus. The singlet ground state recovered through a clean first-order process affording a triplet lifetime of nearly 100 μs. While this is due at low fullerene concentration and low laser power, the kinetics become, however, more complicated at higher fullerene concentration and

higher laser power. In particular, they are affected by efficient i) triplet–triplet and ii) triplet–ground state annihilation processes. This is in agreement with previous studies.[27, 28]

The liquid-crystalline material **1** shows, upon a 18 ps laser pulse, formation of the same 920 nm absorption seen for **7** (see above). In contrast to the slow ISC kinetics ($6.5 \times 10^8\ s^{-1}$), the singlet excited state absorption decays rather rapidly with rate constants typically ranging between $9.8 \times 10^8\ s^{-1}$ (toluene) and $2.0 \times 10^9\ s^{-1}$ (benzonitrile). Importantly, no spectral evidence is found on the picosecond time-scale (i.e., up to 6000 ps) that resembles the triplet absorption around 720 nm, namely the product of the ordinary ISC. Instead, in the monitored wavelength region (500 and 960 nm), a very broadly absorbing transient was found.

With the scope to monitor the full spectral range (UV, visible and NIR), especially the range characteristic for the fullerene π-radical anion absorption around 400 nm and 1040 nm, complementary nanosecond experiments seemed necessary.[27] However, differential absorption changes recorded immediately after a 6 ns laser pulse of **1** in deoxygenated toluene showed no characteristic absorption at all. This suggests that the low solvent polarity is an insufficient means to stabilize the initially formed charge-separated radical pair and that rapid charge recombination prevails on a faster time scale.

Solvents with a higher dielectric constant, such as benzonitrile or DMF, should be potent enough to prevent the fast charge recombination. Indeed, differential absorption changes following the 337 nm laser excitation of **1** in benzonitrile show maxima at 400 and 1040 nm in the visible and NIR regions, respectively. Especially, the NIR maximum is a clear fingerprint absorption of the one-electron reduced fullerene, which suggests the formation of the charge-separated radical pair (Figure 14). On the other hand, no spectral

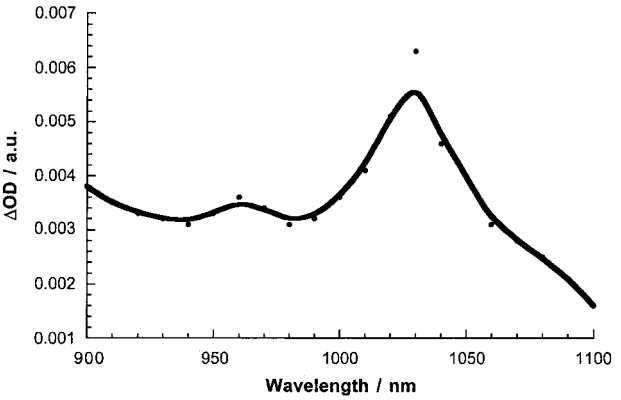

Figure 14. Difference absorption spectrum, recorded following 337 nm laser pulse excitation of **1** ($\approx 5.0 \times 10^{-5}$ M) in deoxygenated benzonitrile in the NIR region, showing the fullerene radical anion. The spectrum was recorded at a delay of 50 ns.

identification can be made for the one-electron oxidized form of ferrocene, since it shows only a very weak absorption maximum at 625 nm ($\varepsilon = 500\ L\,mol^{-1}\,cm^{-1}$).[29]

In addition, the fullerene π-radical anion absorption is a meaningful probe for determining the lifetime of the charge-separated state. From the corresponding decay kinetics, we derived lifetimes of 115, 420 and 27 ns in oxygen-free benzonitrile ($\varepsilon = 24.8$), in an oxygen-free mixture of benzonitrile/DMF (1:1 *v*/*v*) ($\varepsilon = 30.8$) and in oxygen-free CH_2Cl_2 ($\varepsilon = 9.08$), respectively.

To elucidate a possible energy transfer mechanism, the excited state energies of the ferrocene unit should be considered and compared to those of the C_{60} unit (Figure 15).

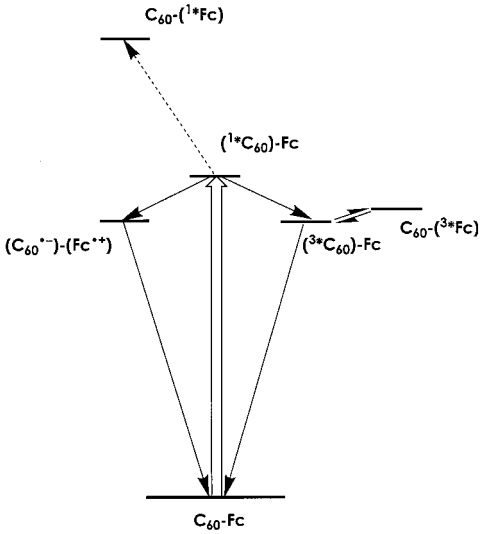

Figure 15. Energy diagram illustrating the different deactivation channels following the photoexcitation of **1**.

The ferrocene singlet excited state (≈ 2.46 eV)[30] is sufficiently separated from the fullerene singlet excited state (1.77 eV) to render a singlet–singlet excited state transfer from the photoexcited C_{60} endothermic and, therefore, unlikely to occur. In contrast, the low-lying ferrocene triplet excited state (1.64 eV)[31] opens, in principle, the opportunity for an energy transfer but only in the form of a singlet–triplet transfer. The C_{60} triplet excited state (1.50 eV), on the other hand, could only intereact with the ferrocene unit *via* a possible equilibrium, which would lead, nonetheless, to a minor population of the ferrocene triplet excited state ($\approx 0.5\,\%$).

The optical characterization of the charge-separated radical pair ($\lambda_{max} \approx 400$ and ≈ 1040 nm) speaks definitively against an energy transfer mechanism. Furthermore, the solvent dependence (Table 3) cannot be explained by a simple energy transfer. In particular, it should be taken into account that the excited state energies remain nearly constant in solvents of different polarities. This, in turn, leads to no significant variations in the free energy changes, for example, between a reaction in non-polar toluene and polar benzonitrile. Thus, intramolecular energy changes should proceed with the same dynamics. Conversely, the energy of the charge-separated radical pair is strongly solvent dependent, with its highest and lowest energies in non-polar and polar solvents, respectively. From the data collected in Table 3, we conclude that the noted solvent dependence is a crucial argument in favor of an electron transfer mechanism rather than an energy transfer mechanism.

Decisive support for an electron transfer mechanism, as the major deactivation pathway of the C_{60} singlet excited state, comes from the energy of the charge-separated radical pair. The latter is, for instance, 1.53 eV in CH_2Cl_2 considering the

  0947-6539/01/0712-2602 $ 17.50+.50/0 *Chem. Eur. J.* **2001**, *7*, No. 12

reduction potential of the fullerene unit (-0.57 V vs SCE)[32] and the oxidation potential of the ferrocene unit ($+0.96$ V vs SCE).[33] In other words, a significantly larger driving force exists for the electron transfer ($-\Delta G_{\text{electron transfer}} = 0.24$ eV) relative to the energy transfer ($-\Delta G_{\text{energy transfer}} = 0.13$ eV), and note that $-\Delta G_{\text{electron transfer}}$ further increases in polar benzonitrile.

Conclusion

Photoinduced intramolecular electron transfer was observed in organic solvents for a fullerene–ferrocene liquid-crystalline material. This observation is of interest for the development of photo-active molecular switches based on the photophysical properties of C_{60}. The role of each subunit (i.e., cholesterol, ferrocene, and fullerene) for governing the supramolecular organization within the liquid-crystalline phases could be understood. This will allow the design of new structures with tailor-made liquid-crystalline and photophysical properties. In the smectic A phase, a relative order with microsegregation of the different units (ferrocene, fullerene and cholesterol) was observed. This order might be important to control the electron transfer processes upon light irradiation. Studies in solution reveal that the ferrocene–fullerene system does indeed give rise to intramolecular electron transfer with relatively long-lived charge-separated species. It is then expected that in the pure liquid-crystalline phase or in liquid-crystalline phases obtained by dissolution of the dyad in liquid crystal solvents (such as E7) control of electron-transfer rates should be achieved. Experiments addressing these issues are currently underway.

Experimental Section

Materials: Toluene (NaH), CH_2Cl_2 ($MgSO_4$, then P_2O_5) and THF (KOH, then Na/benzophenone) were dried and distilled under nitrogen prior to use. [60]Fullerene (99.5 %) was purchased from Southern Chemical Group (Georgia, USA). 1-[10-{4-[(Cholest-5-en-3β-yloxy)carbonyl]phenoxy}-decyloxycarbonyl]-1′-[4-(hydroxyphenoxy)carbonyl]ferrocene[13] (**2**) and cholesteryl 4-hydroxybenzoate[20] (**6**) were synthesized as described in the literature.

Techniques: Column chromatography: silica gel 60 (0.060–0.200 mm, SDS). Transition temperatures (onset point) and enthalpies were determined with a differential scanning Mettler DSC 30 calorimeter connected to a Mettler TA 4000 processor, under N_2, at a rate of $10\,^{\circ}\text{C}\,\text{min}^{-1}$; data treatment used Mettler TA72.2/.5 GRAPHWARE. Optical studies were conducted using a Zeiss-Axioscop polarizing microscope equipped with a Linkam-THMS-600 variable-temperature stage, under N_2. ^{1}H NMR spectra were recorded on a Varian GEMINI 200 spectrometer or a Bruker AMX 400 spectrometer, with the solvent as an internal standard. Elemental analyses were done by the Mikroelementaranalytisches Laboratorium ETH-Zürich.

X-ray diffraction studies: X-ray patterns were recorded on samples filled in Lindemann glass capillaries with two setups based on focalized linear $Cu_{K\alpha 1}$ beams produced with sealed tubes and bent quartz monochromators. The patterns were systematically recorded as a function of temperature by using a home-made oven which is controlled by an INSTEC unit (residual temperature fluctuations of $\pm 0.02\,^{\circ}$C) and an INEL CPS 120 counter. For a better signal-background ratio, long-time patterns were registered at several temperatures on KODAK scientific imaging films with a second setup equipped with a home-made vacuum stand alone oven (residual temperature fluctuations of $\pm 1\,^{\circ}$C). The films were scanned using an EPSON GT-7000 scanner and the images background corrected and integrated in order to get the diffracted intensity as a function of the diffracted angle.

Dilatometry experiments: The technique used to measure the molar volume as a function of temperature was developed by Kovacs[34] for the study of polymers, and afterwards applied to liquid crystals.[35] The measurements were performed with a high precision home-built apparatus, automatically computer controlled, including data acquisition and temperature control ($\pm 0.03\,^{\circ}$C).

Photophysical studies: Picosecond laser flash photolysis were carried out with 355 nm laser pulses from a mode-locked, Q-switched Quantel YG-501 DP (Continuum) Nd/YAG laser system (pulse width ca. 18 ps, 2–3 mJ per pulse). Passing the fundamental output through a D_2O/H_2O solution generated the white continuum picosecond probe pulse.

Nanosecond laser flash photolysis experiments were performed with laser pulses from a Molectron UV-400 (Laser photonics; PRA Model UV-24) nitrogen laser system (337.1 nm, 8 ns pulse width, 1 mJ per pulse) in a front face excitation geometry. The photomultiplier output was digitized with a Tektronix 7912 AD programmable digitizer.

Absorption spectra were recorded with a Milton Roy Spectronic 3000 Array spectrophotometer.

Fluorescence spectra were measured at room temperature with a SLM/Aminco 8100 Spectrofluorometer (Spectronic Instruments). A 570 nm long-pass filter in the emission pass was used in order to eliminate the interference from the solvent and stray light. Long integration times (20 s) and low increments (0.1 nm) were applied. The slits were 2 and 8 nm. Each spectrum was an average of at least five individual scans.

Synthesis

Compound 3: A mixture of 6-bromohexanol (0.40 mL, 3.06 mmol), **2** (2.45 g, 2.42 mmol), K_2CO_3 (2.00 g, 14.47 mmol), acetone (180 mL), and THF (20 mL) was stirred at 60 °C for 24 h. The mixture was cooled to room temperature and filtered. The solid residue was washed with acetone. The organic solvents were combined and evaporated to dryness. Purification of the solid residue by CC (CH_2Cl_2/AcOEt 20:1) and precipitation (dissolution in CH_2Cl_2 and precipitation by pouring the solution into CH_3OH) gave pure **3** (0.98 g, 36 %). ^{1}H NMR (200 MHz, $CDCl_3$): $\delta = 7.98$ (d, 2H, ArH), 7.13 (d, 2H, ArH), 6.92 (d, 2H, ArH), 6.89 (d, 2H, ArH), 5.41 (d, 1H, CH=C, chol), 4.95 (t, 2H, HCp), 4.90 (t, 2H, HCp), 4.85–4.80 (br m, 1H, CHO, chol), 4.51–4.48 (m, 4H, HCp), 4.20 (t, 2H, $CpCO_2CH_2$), 3.99 (t, 2H, CH_2OPh), 3.97 (t, 2H, CH_2OPh), 3.71–3.62 (m, 2H, CH_2OH), 2.45 (d, 2H, chol), 1.95–0.66 (65H, chol, $(CH_2)_8$, $(CH_2)_4$); elemental analysis calcd (%) for $C_{68}H_{94}FeO_9$ (1111.33): C 73.49, H 8.53; found: C 73.50, H 8.39.

Compound 4: A solution of malonyl chloride (44.0 mg, 0.31 mmol) in CH_2Cl_2 (10 mL) was added dropwise to a solution of **3** (0.77 g, 0.69 mmol) and triethylamine (71.0 mg, 0.70 mmol) in CH_2Cl_2 (80 mL). The mixture was stirred at room temperature for 2 h and evaporated to dryness. Purification of the solid residue by CC (CH_2Cl_2/AcOEt 20:1) and precipitation (dissolution in CH_2Cl_2 and precipitation by pouring the solution into ligroin) gave pure **4** (0.55 g, 77 %). ^{1}H NMR (200 MHz, $CDCl_3$): $\delta = 7.97$ (d, 4H, ArH), 7.12 (d, 4H, ArH), 6.92 (d, 4H, ArH), 6.89 (d, 4H, ArH), 5.42 (d, 2H, CH=C, chol), 4.95 (t, 4H, HCp), 4.90 (t, 4H, HCp), 4.85–4.80 (br m, 2H, CHO, chol), 4.51–4.48 (m, 8H, HCp), 4.20/4.17 (2t, 8H, $CpCO_2CH_2$, $H_2CO_2CCH_2CO_2CH_2$), 3.99 (t, 4H, CH_2OPh), 3.96 (t, 4H, CH_2OPh), 3.39 (s, 2H, $O_2CCH_2CO_2$), 2.45 (d, 4H, chol), 2.05–0.69 (130H, chol, $(CH_2)_8$, $(CH_2)_4$); ^{13}C NMR (50 MHz, $CDCl_3$): $\delta = 170.43$, 169.48, 166.73, 165.84, 162.84, 156.74, 144.26, 139.84, 131.56, 123.06, 122.69, 122.55, 115.07, 114.00, 74.22, 73.49, 73.31, 72.89, 72.05, 71.96, 71.76, 68.21, 65.56, 64.75, 56.75, 56.18, 50.11, 42.37, 41.70, 39.81, 39.57, 38.35, 37.11, 36.71, 36.24, 35.86, 31.95, 29.52, 29.40, 29.31, 29.23, 28.85, 28.49, 28.31, 28.07, 26.03, 25.78, 25.69, 24.36, 23.88, 22.88, 22.63, 21.12, 19.44, 18.79, 11.93; elemental analysis calcd (%) for $C_{139}H_{188}Fe_2O_{20}$ (2290.70): C 72.88, H 8.27; found: C 72.92, H 8.24.

Compound 1: A solution of DBU (1M, 0.27 mL, 0.27 mmol) was added dropwise to a solution of C_{60} (98 mg, 0.136 mmol), **4** (310 mg, 0.135 mmol) and iodine (35 mg, 0.138 mmol) in toluene (100 mL). The mixture was stirred at room temperature for 3 h and evaporated to dryness. Purification of the solid residue by CC (toluene, then toluene/AcOEt 20:1) and precipitation (dissolution in toluene and precipitation by pouring the solution into CH_3OH) gave pure **1** (140 mg, 34 %). ^{1}H NMR (400 MHz, $CDCl_3$): $\delta = 7.97$ (d, 4H, ArH), 7.11 (d, 4H, ArH), 6.91 (d, 4H, ArH), 6.88 (d, 4H, ArH), 5.41 (d, 2H, CH=C, chol), 4.94 (t, 4H, HCp), 4.89 (t, 4H, HCp), 4.88–4.80 (br m, 2H, CHO, chol), 4.52 (t, 4H, $C_{60}CO_2CH_2$), 4.50–

4.47 (m, 8H, HCp), 4.19 (t, 4H, $CpCO_2CH_2$), 3.98 (t, 4H, CH_2OPh), 3.96 (t, 4H, CH_2OPh), 2.44 (d, 4H, chol), 2.03 – 0.68 (130H, chol, $(CH_2)_8$, $(CH_2)_4$); ^{13}C NMR (100 MHz, $CDCl_3$): $\delta = 170.35$, 169.39, 165.77, 163.65, 162.76, 156.63, 145.31, 145.23, 145.14, 145.11, 144.85, 144.65, 144.59, 144.21, 143.85, 143.06, 142.98, 142.96, 142.17, 141.85, 140.93, 139.75, 138.94, 131.48, 122.98, 122.63, 122.49, 114.99, 113.93, 74.14, 73.39, 73.23, 72.82, 71.97, 71.86, 71.68, 68.13, 68.08, 67.30, 64.67, 56.66, 56.10, 52.39, 50.01, 42.29, 39.71, 39.49, 38.27, 37.03, 36.63, 36.15, 35.77, 31.91, 31.85, 29.44, 29.31, 29.22, 29.09, 28.77, 28.54, 28.21, 27.98, 27.92, 25.95, 25.83, 25.74, 24.26, 23.80, 22.79, 22.53, 21.02, 19.36, 18.69, 11.84; elemental analysis calcd (%) for $C_{199}H_{186}Fe_2O_{20}$ (3009.34): C 79.43, H 6.23; found: C 79.37, H 6.21.

Compound 5 ($n = 8$): A mixture of 1-bromooctane (1.14 g, 5.90 mmol), cholesteryl 4-hydroxybenzoate (2.00 g, 3.95 mmol), K_2CO_3 (2.72 g, 16.68 mmol), DMF (40 mL), and THF (20 mL) was stirred under reflux for 20 h, cooled to room temperature and filtered. The solid residue was washed with THF. The organic solvents were combined and evaporated to dryness. Purification of the solid residue by CC (CH_2Cl_2) and crystallization (CH_2Cl_2/EtOH) gave pure **5** ($n = 8$) (1.90 g, 78%). ^1H NMR (200 MHz, $CDCl_3$): $\delta = 7.98$ (d, 2H, ArH), 6.90 (d, 2H, ArH), 5.43 (d, 1H, CH=C, chol), 4.86 – 4.80 (br m, 1H, CHO, chol), 4.01 (t, 2H, CH_2OPh), 2.44 (d, 2H, chol), 2.06 – 0.69 (56H, chol, $CH_3(CH_2)_6$); elemental analysis calcd (%) for $C_{42}H_{66}O_3$ (618.98): C 81.50, H 10.75; found: C 81.26, H 10.63.

Compounds **5** ($n = 12$, 14) were prepared by analogy to the above procedure from 1-bromododecane [→ **5** ($n = 12$)] or 1-bromotetradecane [→ **5** ($n = 14$)]. The analytical data are in agreement with their structure.

Acknowledgements

The Swiss National Science Foundation and the French-Swiss international program of scientific collaboration PICS No 742 CNRS are gratefully acknowledged for their financial support. Part of this work was supported by the Office of Basic Energy Science of the US Department of Energy; this is contribution NDRL 4284 from Notre Dame Radiation Laboratory.

[1] a) M. Prato, *J. Mater. Chem*. **1997**, *7*, 1097; b) M. Prato, *Top. Curr. Chem.* **1999**, *199*, 173.

[2] a) K. E. Geckeler, A. Hirsch, *J. Am. Chem. Soc.* **1993**, *115*, 3850; b) C. J. Hawker, *Macromolecules* **1994**, *27*, 4836; c) C. Weiss, C. Friedrich, R. Mülhaupt, H. Frey, *Macromolecules* **1995**, *28*, 403; d) B. Liu, E. Bunker, Y.-P. Sun, *Chem. Commun*. **1996**, 1241; e) Y.-P. Sun, B. Liu, D. K. Moton, *Chem. Commun*. **1996**, 2699; f) Y. Ederle, C. Mathis, *Macromolecules* **1997**, *30*, 4262; g) H. Okamura, N. Ide, M. Minoda, K. Komatsu, T. Fukuda, *Macromolecules* **1998**, *31*, 1859; h) Z. Y. Wang, L. Kuang, X. S. Meng, J. P. Gao, *Macromolecules* **1998**, *31*, 5556; i) L. Dai, A. W. H. Mau, X. Zhang, *J. Mater. Chem*. **1998**, *8*, 325; j) A. Kraus, K. Müllen, *Macromolecules* **1999**, *32*, 4214.

[3] a) K. L. Wooley, C. J. Hawker, J. M. J. Fréchet, F. Wudl, G. Srdanov, S. Shi, M. Kao, *J. Am. Chem. Soc*. **1993**, *115*, 9836; b) C. J. Hawker, K. L. Wooley, J. M. J. Fréchet, *J. Chem. Soc. Chem. Commun*. **1994**, 925; c) X. Camps, H. Schönberger, A. Hirsch, *Chem. Eur. J.* **1997**, *3*, 561; d) F. Cardullo, F. Diederich, L. Echegoyen, T. Habicher, N. Jayaraman, R. M. Leblanc, J. F. Stoddart, S. Wang, *Langmuir* **1998**, *14*, 1955; e) M. Brettreich, A. Hirsch, *Tetrahedron Lett*. **1998**, *39*, 2731; f) N. Armaroli, C. Boudon, D. Felder, J.-P. Gisselbrecht, M. Gross, G. Marconi, J.-F. Nicoud, J.-F. Nierengarten, V. Vicinelli, *Angew. Chem*. **1999**, *111*, 3895; *Angew. Chem. Int. Ed*. **1999**, *38*, 3731; g) J.-F. Nierengarten, D. Felder, J.-F. Nicoud, *Tetrahedron Lett*. **1999**, *40*, 269; h) J.-F. Nierengarten, D. Felder, J.-F. Nicoud, *Tetrahedron Lett*. **1999**, *40*, 273; i) J.-F. Nierengarten, D. Felder, J.-F. Nicoud, *Tetrahedron Lett*. **2000**, *41*, 41; j) J.-F. Nierengarten, *Chem. Eur. J.* **2000**, *6*, 3667.

[4] a) M. Maggini, G. Scorrano, M. Prato, G. Brusatin, P. Innocenzi, M. Guglielmi, A. Renier, R. Signorini, M. Meneghetti, R. Bozio, *Adv. Mater*. **1995**, *7*, 404; b) R. Signorini, M. Zerbetto, M. Meneghetti, R. Bozio, M. Maggini, C. De Faveri, M. Prato, G. Scorrano, *Chem. Commun*. **1996**, 1891; c) M. Maggini, C. De Faveri, G. Scorrano, M. Prato, G. Brusatin, M. Guglielmi, M. Meneghetti, R. Signorini, R. Bozio, *Chem. Eur. J.* **1999**, *5*, 2501; d) A. Kraus, M. Schneider, A. Gügel, K. Müllen, *J. Mater. Chem*. **1997**, *7*, 763.

[5] a) M. Hetzer, S. Bayerl, X. Camps, O. Vostrowsky, A. Hirsch, T. M. Bayerl, *Adv. Mater*. **1997**, *9*, 913; b) M. Hetzer, H. Clausen-Schaumann, S. Bayerl, T. M. Bayerl, X. Camps, O. Vostrowsky, A. Hirsch, *Angew. Chem*. **1999**, *111*, 2103; *Angew. Chem. Int. Ed.* **1999**, *38*, 1962; c) M. Breittreich, S. Burghardt, S. Böttcher, T. Bayerl, S. Bayerl, A. Hirsch, *Angew. Chem*. **2000**, *112*, 1915; *Angew. Chem. Int. Ed*. **2000**, *39*, 1845.

[6] D. M. Guldi, *Chem. Commun*. **2000**, 321.

[7] H. Imahori, Y. Sakata, *Eur. J. Org. Chem*. **1999**, 2445.

[8] a) N. S. Sariciftci, L. Smilowitz, A. J. Heeger, F. Wudl, *Science* **1992**, *258*, 1474; b) L. Pasimeni, A. L. Maniero, M. Ruzzi, M. Prato, T. Da Ros, G. Barbarella, M. Zambianchi, *Chem. Commun*. **1999**, 429.

[9] G. Yu, J. Gao, J. C. Hummelen, F. Wudl, A. J. Heeger, *Science*, **1995**, *270*, 1789; b) J.-F. Nierengarten, J.-F. Eckert, J.-F. Nicoud, L. Ouali, V. Krasnikov, G. Hadziioannou, *Chem. Commun*. **1999**, 617.

[10] K. Hutchison, J. Gao, Y. Rubin, F. Wudl, *J. Am. Chem. Soc*. **1999**, *121*, 5611.

[11] T. Chuard, R. Deschenaux, *Helv. Chim. Acta* **1996**, *79*, 736.

[12] R. Deschenaux, M. Even, D. Guillon, *Chem. Commun*. **1998**, 537.

[13] B. Dardel, R. Deschenaux, M. Even, E. Serrano, *Macromolecules* **1999**, *32*, 5193.

[14] T. Chuard, R. Deschenaux, A. Hirsch, H. Schönberger, *Chem. Commun*. **1999**, 2103.

[15] a) C. Bingel, *Chem. Ber*. **1993**, *126*, 1957; b) J.-P. Bourgeois, F. Diederich, L. Echegoyen, J.-F. Nierengarten, *Helv. Chim. Acta* **1998**, *81*, 1835.

[16] N. Tirelli, F. Cardullo, T. Habicher, U. W. Suter, F. Diederich, *J. Chem. Soc. Perkin Trans. 2* **2000**, 193.

[17] D. Felder, B. Heinrich, D. Guillon, J.-F. Nicoud, J.-F. Nierengarten, *Chem. Eur. J.* **2000**, *6*, 3501.

[18] a) R. Deschenaux, M. Schweissguth, A.-M. Levelut, *Chem. Commun*. **1996**, 1275; b) R. Deschenaux, M. Schweissguth, M.-T. Vilches, A.-M. Levelut, D. Hautot, G. L. Long, D. Luneau, *Organometallics* **1999**, *18*, 5553.

[19] D. M. Guldi, M. Maggini, G. Scorrano, M. Prato, *J. Am. Chem. Soc*. **1997**, *119*, 974.

[20] R. Deschenaux, C. Masoni, H. Stoeckli-Evans, S. Vaucher, J. Ketterer, R. Steiger, A. L. Weisenhorn, *J. Chem. Soc. Dalton Trans.* **1994**, 1051.

[21] U. Jonas, F. Cardullo, P. Belik, F. Diederich, A. Gügel, E. Harth, A Hermann, L. Isaacs, K. Müllen, H. Ringsdorf, C. Thielgen, P. Uhlmann, A. Vasella, C. A. A. Waldraff, M. Walter, *Chem. Eur. J.* **1995**, *1*, 243.

[22] D. Guillon, A. Skoulios, *J. de Physique* **1976**, *37*, 797.

[23] R. Deschenaux, I. Jauslin, U. Scholten, F. Turpin, D. Guillon, B. Heinrich, *Macromolecules* **1998**, *31*, 5647.

[24] D. Guillon,. A. Skoulios, *Mol. Cryst. Liq. Cryst*. **1977**, *39*, 31.

[25] P. Seurin, D. Guillon, A. Skoulios, *Mol. Cryst. Liq. Cryst*. **1980**, *61*, 185.

[26] G. Poeti, E. Fanelli, G. Torquati, D. Guillon, *Il Nuovo Cimento*, *Series 1*, *Vol. 2D*, **1983**, 1335.

[27] a) D. M. Guldi, H. Hungerbühler, K.-D. Asmus, *J. Phys. Chem*. **1995**, *99*, 9380; b) D. M. Guldi, K.-D. Asmus, *J. Phys. Chem. A*. **1997**, *101*, 1472; c) D. M. Guldi, M. Prato, *Acc. Chem. Res.* **2000**, *33*, 695.

[28] a) T. W. Ebbesen, K. Tanigaki, S. Kuroshima, *Chem. Phys. Lett*. **1991**, *181*, 501; b) N. M. Dimitrijevic, P. V. Kamat, *J. Phys. Chem*. **1992**, *96*, 4811; c) R. B. Weisman in *Optical and Electronical Properties of Fullerenes and Fullerene-based Materials* (Eds.: J. Shinar, Z. V. Vardeny), Marcel Dekker, New York, **2000**, pp. 83 – 117.

[29] M. Faraggi, D. Weinraub, F. Broitman, M. R. DeFelippis, M. H. Klapper, *Radiat. Phys. Chem*. **1988**, *32*, 293.

[30] Y. S. Sohn, D. N. Hendrickson, H. B. Gray, *J. Am. Chem. Soc*. **1971**, *93*, 3603.

[31] W. G. Herkstroeter, *J. Am. Chem. Soc.* **1975**, *97*, 4161.

[32] E. Dietel, A. Hirsch, J. Zhou, A. Rieker, *J. Chem. Soc. Perkin Trans. 2* **1998**, 1357.

[33] We thank Prof. Francesco Paolucci for providing these data to us.

[34] A. J. Kovacs, *Ric. Sci. Suppl*. **1955**, *25*, 668.

[35] D. Guillon, PhD thesis, University of Strasbourg, 1976; D. Guillon, A. Skoulios, *R. Acad. Sci. Paris* **1974**, *C278*, 1974.

Received: December 4, 2000 [F2910]

